Draft version August 4, 2016
Preprint typeset using LaTeX style emulateapj v. 12/16/11
1 2
doi:10.1073/pnas.1523583113

HIGH-FREQUENCY OSCILLATIONS IN HUMAN AND MONKEY NEOCORTEX DURING THE WAKE-SLEEP CYCLE

Michel Le Van Quyen †[1] Lyle E. Muller †[2] Bartosz Telenczuk †[3] Eric Halgren [4]
Syd S. Cash [5] Nicholas G. Hatsopoulos [6] Nima Dehghani ¶[7,8] Alain Destexhe ¶[3]
1. Centre de Recherche de l'Institut du Cerveau et de la Moelle pinire (CRICM), UPMC, France.
2. Computational Neurobiology Laboratory, Salk Institute, La Jolla, USA.
3. Laboratory of Computational Neuroscience, Unit de Neurosciences, Information et Complexit, CNRS, France.
4. Multimodal Imaging Laboratory, Departments of Neurosciences and Radiology, University of California San Diego, USA.
5. Department of Neurology, Massachusetts General Hospital and Harvard Medical School, USA.
6. Department of Organismal Biology and Anatomy, Committee on Computational Neuroscience, University of Chicago, USA.
7. Wyss Institute for Biologically Inspired Engineering, Harvard University, USA.
8. New England Complex Systems Institute, Cambridge, USA.

Draft version August 4, 2016

ABSTRACT

Beta (β) and Gamma (γ) oscillations are present in different cortical areas and are thought to be inhibition-driven, but it is not known if these properties also apply to γ oscillations in humans. Here, we analyze such oscillations in high-density microelectrode array recordings in human and monkey during the wake-sleep cycle. In these recordings, units were classified as excitatory and inhibitory cells. We find that γ oscillations in human and β oscillations in monkey are characterized by a strong implication of inhibitory neurons, both in terms of firing rate, and in their phasic firing with the oscillation cycle. β and γ waves systematically propagate across the array, with similar velocities, during both wake and sleep. However, only in slow-wave sleep (SWS), β and γ oscillations are associated with highly coherent and functional interactions across several millimeters of the neocortex. This interaction is specifically pronounced between inhibitory cells. These results suggest that inhibitory cells are dominantly involved in the genesis of β and γ oscillations, as well as in the organization of their large-scale coherence in the awake and sleeping brain. The highest oscillation coherence found during slow-wave sleep suggests that fast oscillations implement a highly-coherent reactivation of wake patterns, which may support memory consolidation during slow-wave sleep.

Subject headings: Excitation | Inhibition | State-dependent firing | Wave propagation | Synchrony

SIGNIFICANCE

We show in humans, that in comparison with excitatory cells, inhibitory neurons have a stronger spiking activity during γ oscillations in wake-sleep cycle. During β oscillations in monkey neocortex, inhibitory cells show a more active firing. Unlike excitatory cells, inhibitory cells show correlations during slow-wave sleep fast oscillations over several millimeters in neocortex. During both wake and sleep, β and γ waves systematically propagate with a dominant trajectory across the array with similar velocities. These findings suggest that inhibition-driven β and γ oscillations may contribute to the reactivation of information during sleep through orchestrating highly coherent spiking activity patterns.

INTRODUCTION

Neocortical Beta (β) and Gamma (γ) oscillations have been largely studied in the context of action/cognition during wakefulness (1; 2; 3). Though numerous studies have focused intensely on the information processing role of β and γ during wakefulness, these rhythms do also occur during deep anesthesia and natural sleep (4; 5; 6). Additionally, while very high-frequency allocortical oscillations (such as ripples 80-200 Hz and fast ripples 200-500 Hz in rodent/human hippocampus) have been thoroughly implicated in sleep-dependent memory consolidation (see (7) and reviews (8; 9)), the occurrence and role of neocortical β and γ oscillations during sleep remains largely unexplored and their studies have been limited to macroscopic (whole-brain) scales (such as (10)). A recent study, using microwires and intracranial EEG recordings in the neocortex of epileptics, has verified the strong presence of γ oscillations during slow-wave sleep (SWS) (11). That study also showed a marked increase of spiking during γ, a suggestive indicator of association with cortical UP states. Here, we evaluate the presence of neocortical β and γ oscillations during the wake-sleep cycle at the level of local circuitry using dense two-dimensional multielectrode recordings with identified excitatory and inhibitory cells (12; 13).

Experimental and theoretical studies suggest that thalamocortical oscillations (including β and γ) are generated through a combination of intrinsic mechanisms involving the interplay between different ionic currents and extrinsic interaction of inhibitory and excitatory cell populations (14). Mechanistically, it has been shown that the temporal interplay of synaptic excitation and inhibition (15) and the dynamic balance of ensemble excitation and inhibition (13) shape the neocortical network activity during different states (wakefulness, slow-wave sleep and rapid-eye movement). Specifically, studies of hip-

[1] cite as Le Van Quyen et al. Proc. Natl. Acad. Sci. U.S.A., 2016,doi = 10.1073/pnas.1523583113

[2] †co-first, ¶: corresponding author. M.L.V.Q., N.D., and A.D. designed research; E.H., S.C., and N.G.H. performed experiments; M.L.V.Q., L.E.M., B.T., and N.D. analyzed data; and N.D. and A.D. wrote the paper.
nima.dehghani@wyss.harvard.edu, destexhe@unic.cnrs-gif.fr

pocampal and enthorhinal cortex point to a link between phasic discharge of fast-spiking interneurons and γ cycle (16; 17; 18; 19) and show how the excitation-inhibition balance modulates γ oscillations (20). Both experimental and simulation studies frame β oscillations as inhibition-based rhythms as well (21; 22). Here, we show how the interplay of neocortical inhibitory (fast-spiking, FS) and excitatory (regular-spiking, RS) activity are related to these oscillations during sleep-wake cycle. Additionally, we examine the spiking relation with LFP (local field potential) to better elucidate the spatiotemporal organization of inhibitory/excitatory spiking during neocortical β and γ wave propagation and coherence in the sleep-wake cycle.

RESULTS

In what follows, first, we examine how excitatory and inhibitory units correlate with γ and β oscillations. Next, we analyze their their spatial coherence and spatiotemporal organization, comparing wake and sleep states.

PROMINENT PRESENCE OF HIGH FREQUENCY OSCILLATIONS DURING THE WAKE-SLEEP CYCLE

In both man and monkey, we detected numerous γ and β oscillatory events in multielectrode recordings during both wakefulness and sleep states (see Fig.1 and Fig.S1). In both raw and filtered signal (β and γ range), large-amplitude fast and transient oscillations appeared in many channels as discrete events which were clearly distinguishable from background activity (see Table S1). In the temporal neocortex of humans, γ (30-50 Hz) was the main high frequency oscillatory event with similar dominant frequencies and inter-episode intervals across all stages of vigilance (see Table S1). In monkey premotor (PMd) and motor (MI) neocortical recordings, β (15-30 Hz) was the prominent high frequency oscillation with similar properties across Sleep-Wake cycle (see Table S2). For individual examples of β and γ events, see supplementary figures (Figs. S2 and S3).

FIRING PROBABILITY OF FS AND RS CELLS IN RELATION TO β AND γ

After categorizing the cells into the two fast-spiking (FS) inhibitory and regular-spiking (RS) excitatory groups, we tested their firing relation with the β and γ oscillations in wake and sleep states. During both β and γ events, a larger proportion of FS cells showed high firing probability (72% for γ; 65% for β). This higher firing rate during the oscillation was not restricted to FS cells; some RS cells show higher firing probability as well (36% for γ; 32% for β, see Fig.2 heatmaps). Similar firing behaviors were seen across the different stages of vigilance. Firing properties of FS and RS during different states are summarized in Table S3.

HETEROGENEITY OF SPIKING PATTERN DURING β AND γ

Evaluation of firing probability of a given cell across different (β and γ) oscillatory events shows that these cells have a remarkable heterogeneity of response patterns (Fig.2, raster panels). Some cells (either FS or RS, such as 33 and 56 in γ events shown in the left panel

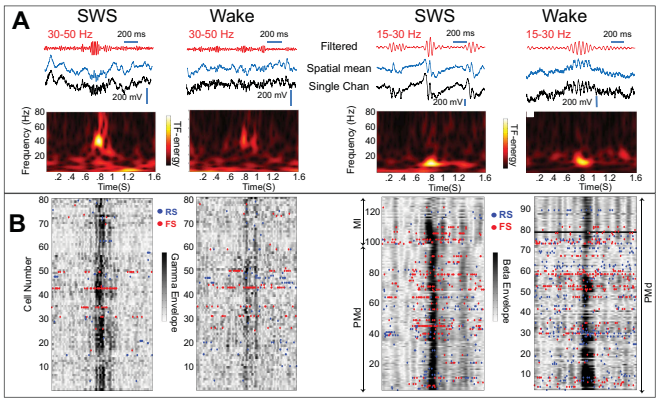

FIG. 1.— **γ and β oscillations during sleep and wakefulness. A)** γ and β oscillations were identified in LFP during slow-wave sleep (SWS) and wakefulness (WAKE) in both human and monkey. Top: Raw and filtered traces , Bottom: Wavelet time-frequency of the sample epoch. **B)** These oscillations most frequently appeared at about the same time across the array, forming broad spatial patterns. Red and blue dots are spiking from inhibitory FS and excitatory RS cells recorded with the same electrodes from which the LFP oscillatory envelope is calculated.

Fig.2) show highly modulated firing rate (with respect to the oscillatory event timing) and some do not show the same stereotypical behavior across different events. Cells that do not show any strong firing changes during the oscillations manifest distinctively different firing patterns. For example, some of these cells show higher firing rate in comparison to the others (such as sparse firing of cells 55 and 57 versus the stochastic but yet higher firing rate of cells 16, 2 and 154 in Fig.2). In summary, both FS and RS cells show heterogeneous patterns of firing, with a larger proportion of FS cells showing higher firing rate during β or γ, either in a tight stereotypical fashion or more variably.

PHASE-LOCKING OF FS AND RS CELLS RELATIVE TO β AND γ

As shown above (Fig.2), firing of FS and RS cells show changes during the oscillatory β and γ events. Extracted phase of the LFP (from the electrode that recorded spiking of a given cell), shows that both FS and RS cells have variable degrees of phase-locking (evaluated with Rayleigh test at $p<0.05$, see Fig.3). The percentage of cells that their firing was phase locked to β and γ oscillations varied in different behavioral states; it was highest during SWS (22% of FS and 6% of RS for γ; 42% of FS and 28% of RS for β) and lowest during wake (13% of FS and 9% of RS for γ; 4% of FS and 2% of RS for β). In all states, in both β and γ, a larger proportion of FS cells exhibited significant phase locking than RS cells. The degree of this phase-locking was variable from cell to cell, with some showing strong stereotypical modulation (such as cell 57 in β oscillation panel of Fig.3A). Note that a given cell does not necessarily show a strict tuning to a given frequency range, but rather may show a stronger relation with higher frequencies, as shown in Fig.S4. Furthermore, in both β and γ, the distribution of the preferential firing phases revealed that significantly modulated FS cells fired earlier than the RS cells ($p = 0.01$, two-sample permutation test; Fig.3C).

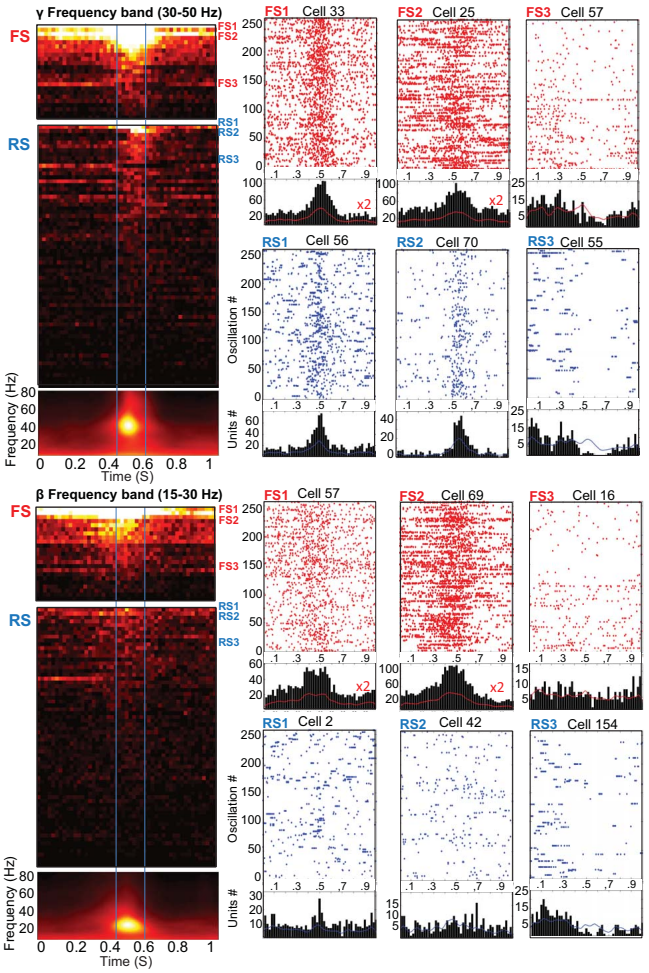

FIG. 2.— **Oscillations-triggered probability density of firing rates for RS and FS neurons.** In each triplet set of heatmaps, the bottom one shows wavelet time-frequency and the top two show FS and RS firing during these example γ and β oscillations. The firing rate is color-coded (black - baseline firing rate; white - 5 standard deviations from the baseline). The cells are ordered by their discharge probability during γ or β oscillations (bin size, 20 ms). A large proportion of FS cells shows increased firing rate during γ and β. Raster panels show spiking patterns of few sample FS and RS cells. In these raster plots, each row is the spiking of the example cell in one (γ or β) oscillatory epoch. The correspondent average firing pattern (rows in the heatmap) for each example cell (FS1, RS2, etc) are indicated along the right edge of the heatmaps. Note the remarkably heterogeneous discharge patterns.

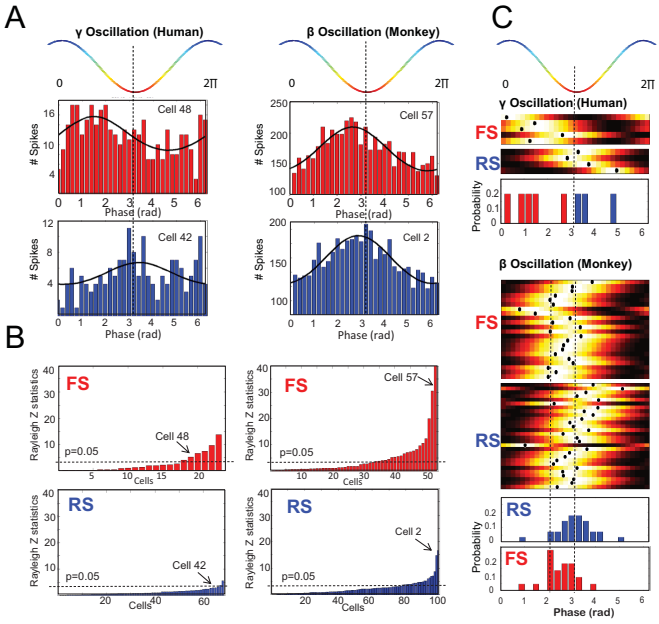

FIG. 3.— **Phase-locking of spikes relative to the field oscillation cycle for RS and FS neurons during SWS.** Phase locking was considered significant if the hypothesis of circular uniformity for its field phase distribution could be rejected at p=0.05 using a Rayleigh statistical test. **A. Phase distributions of several significantly phase-locked RS and FS cells.** The distributions were fitted with a von Mises function here depicted with continuous black lines. rad, radian. **B. Histogram of Rayleigh's Z value for all investigated RS cells (blue) and FS (red).** Note the large proportion of FS cells that were modulated by β and γ patterns. **C. Histogram of preferred firing phase for significantly phase-locked neurons.** For each RS (blue) and FS (red) cells, the normalized distribution is depicted (hot colors) with black dots indicating the preferred firing phase. Note that, on average, FS cells fired earlier than the RS cells.

LARGE-SCALE COHERENCE OF LOCAL FIELD ACTIVITIES AND UNITS DURING β AND γ

Correlations during β and γ oscillations represented as a function of distance displayed marked differences between awake, REM, and SWS (Fig.4.A). During SWS, fast oscillations displayed a remarkable spatiotemporal coherence, as indicated by the high values of spatial correlations for large distances, in contrast with the steeper decline of spatial correlations with distance during waking and REM. While the strong links of spatial correlations were present both during wakefulness and SWS, large patterns of strong links can mostly be seen during SWS (Fig.S5, Fig.S6). The stronger correlation during SWS is further confirmed by the correlation between spikes and LFPs as a function of distance (Fig.4B). This analysis shows that, during SWS, only FS cells expressed a high degree of significant phase-locking with fast field oscillations over large cortical distances (up to 3 mm). In contrast, during wakefulness, attempts to find correlations between the β / γ recorded by one electrode and units recorded by other electrodes were unsuccessful. Finally, considering that some cells show large-scale correlations of their firing with LFPs, we also tested whether they show spike synchrony with each other during β / γ oscillations. During SWS high-frequency oscillations, only FS cells show statistically significant spike synchrony with other FS cells (Fig.4C). Additionally, these strong correlations did not show any distance-dependence. A given cell (such as cell 57 or 69 in the shown example Fig.4D) may show strong synchrony (during oscillatory events) with cells that are distant within the same recording multielectrode array. This synchronous spiking could even extend to other cells recorded in another cortical area (from PMd to M1). By contrast, no such correlations over large distances were present for periods of waking.

OSCILLATORY WAVE PROPAGATION

Local field potentials (LFPs) recorded across the multielectrode arrays showed patterns of traveling waves, in both β and γ oscillatory events during wakefulness, SWS, and REM (Fig.5). These oscillatory traveling waves exhibited speeds ∼500 mm/s and showed repeated stereo-

typical spatiotemporal patterns within a given multielectrode array. Such stereotypical behavior could be reminiscent of an underlying connectivity and/or barrage of directed input and outputs. The relative phase difference of each LFP compared to the global mean, averaged over all detected oscillations, revealed the spatial dynamics of dominant propagating wave directions (Fig.5,A2 and A4). A phase-based approach to detect individual traveling waves identified events with some heterogeneity (see Methods and Supplementary movies 1-3) that generally follow the dominant direction. Both β and γ oscillatory events exhibited similar distributions of phase speed, while δ frequency events exhibited speeds lower by almost an order of magnitude (Fig.5B, left). Identified γ frequency wave events exhibited a similar phase speed distributions across wakefulness, SWS, and REM (Fig.5B, right), indicating possibly similar mechanisms for this wave-like behavior across the functional states of the network.

DISCUSSION

Sleep studies of neocortical β and γ rhythms have been mostly focused on their macroscopic manifestation and grouping of different rhythms (23; 24; 25; 26). It has been shown that coherent γ oscillations are present during REM (rapid eye movement) in MEG (magnetoencephalography) recordings (10). Evidence from extracranial electroencephalography (EEG) and intracranial EEG (iEEG) recordings in epileptics shows that the synchrony of macroscopic γ is lower in SWS (slow-wave sleep) and REM relative to the awake state (27) and that γ presence shows a phasic expression during SWS (11; 28). In this study, we took advantage of high spatial sampling of 10x10 multielectrode arrays in humans and monkeys and further confirmed that β and γ are prominently present during sleep-wake cycle at the level of neocortical micro-circuitry (Fig.1). Our findings show that the transient fast rhythms in wake-sleep are not limited to allocortex and that β and γ are preserved across different neocortical areas (such as temporal, pre-motor and motor studied here). Additionally, we observed a clear heterogeneity of firing patterns in both cell populations during both β and γ (Fig.2). Our results show that the cellular correlates of beta and gamma oscillations implicate both inhibitory and excitatory populations, but with a clear prominence of inhibitory cells.

Theoretically, it has been shown that inhibition plays a dominant role in generating synchrony (29), and is implicated in the large-scale synchronization of oscillations in the thalamocortical system (30). Experimental evidence also points to a more effective γ elicitation through optogenetic stimulation of inhibitory, rather than excitatory cells (31). Regardless, it is still controversial whether fast rhythms such as γ are generated through an exclusive interaction between interneurons (ING, Interneuron Gamma) or via PING (pyramidal-interneuron Gamma; For a detailed account of fast oscillation's cellular mechanisms see (32; 33; 34)). However, the big picture is fairly intricate and involves an array of complex cellular and subcellular mechanisms (22; 33). Nonetheless, while extracellular recordings cannot directly discern mechanisms such as ING vs PING, they can provide a channel to study patterns of ensemble activity during fast rhythms. We observed that even though both inhibitory FS and excitatory RS cells are implicated in β and γ oscillatory events, a larger proportion of inhibitory cells showed higher firing (Fig.3A,B and Table S3). Furthermore, FS cells fired earlier than the RS cells in relation to the oscillatory cycle (Fig.3C). Given that prior experiments suggest cycle-by-cycle recruitment of inhibition after excitation in orchestrating high frequency rhythms (20), it is likely that the origin of the observed fast rhythms in our experiment was either distal to the recorded region/layer or included a mixture of distal and focal elements. These possible distal contributions could be conveyed through afferents from different layers of the involved column or from neighboring areas. In fact, divergent generating mechanisms of fast rhythms, depending on the cortical layer and rhythm frequency range, have been previously explored in models and in vitro preparations (35). Even though our results show a stronger phase-locking with fast oscillations, our experimental preparation does not allow a distinction between focal and likely distal oscillation generators.

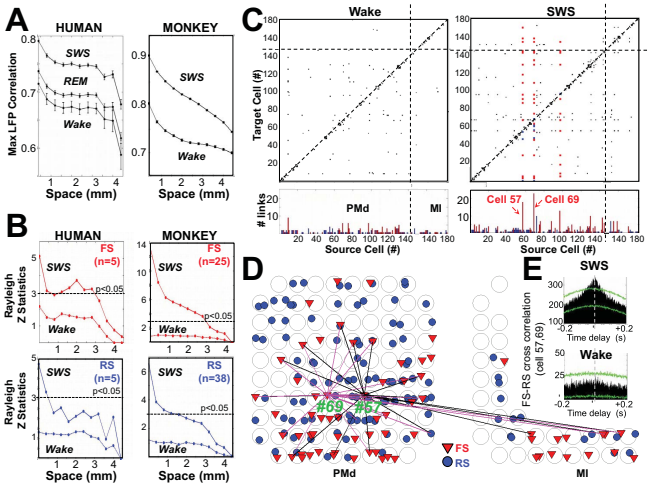

FIG. 4.— **Large-scale coherence of local field potential activities and spikes during wake sleep γ-β oscillations. A: Field-field correlations:** Maximum of the cross-correlation (within a time lag ranging [-50 +50] ms) averaged over all filtered LFPs (in the γ frequency range for human and β for monkey) vs spatial distance. In both human and monkey, fast oscillations displayed locally correlated dynamics in all states but the correlations decline with distance. During SWS, correlations stayed high across cortical distances of several millimeters. **B: Spike-Field correlations:** Averaged Rayleigh's Z value vs distance from LFP sites for all significantly locked RS and FS neurons. During SWS, FS neurons are phase-locked with field over up to 3 millimeters in both human and monkey. This phase-locking disappears during wakefulness. In contrast, RS show less spatial coherence during SWS and no significant correlation with distant LFP sites during wakefulness. **C: Cell-cell correlations:** Matrices of significant spike synchronization for PMd and MI cells during β oscillations in monkey. For SWS, the type of target cells is indicated for cells 57/69 with colors (red=FS, blue=RS). Note that most of the cell-cell interactions over the extent of the array are FS. **D: The spatial distribution of significant cell-cell interactions for two FS cells.** Spike synchrony with cell 57/69 can be seen with cells that are spatially far. This synchronous spiking could even extend to other cells recorded in another cortical area (from PMd to M1). **E: Example of spike cross-correlogram during SWS and wake.** Note the presence of a significant peak around zero during SWS that disappears during the wake state (in green, mean±3 standard deviations of 100 surrogates generated by temporal jittering).

Oscillatory rhythms could coexist, manifest state-dependent variability and act as cell assembly organizers (36; 37). While the exact functional role of oscillations is still a matter of debate, several hypotheses propose they play a role in the representation of information, regulation of the flow of information and, last but not least, storage and retrieval of information in neural circuitry (see review by (38)). These not mutually exclusive roles of oscillations relate rhythms to the general notion of plasticity and memory consolidation during sleep (39; 9; 40; 41). Oscillations exert these effects through coordinating population activity in local and distant neuronal assemblies in slow-wave sleep (SWS) (42). Different synchronization mechanisms of β and γ are thought to be related to distant interaction and local computations during cognition (43). Much emphasis of near zero-phase lag synchrony over a few millimeters has been based on awake cognitive states (44; 45), even though the initial evidence came from anesthetized state experiments (46; 47; 48). However, the synchronization of neighboring cortical sites through fast rhythms is not limited to awake or anesthetized states and it occurs during a range of altered states of consciousness (anesthesia, SWS and REM) (4; 49). Interestingly, we also noted that correlated firings can be detected between spatially distant (PMd and M1) FS neurons (Fig.4).

One of the most striking observation was that the coherence of γ oscillations markedly increases during sleep. At the level of LFPs, we found that the millimeter-scale coherence of fast oscillations is more coherent during REM sleep compared to wakefulness, in agreement with previous studies in MEG (10) and extracellular recordings in cats (6). Interestingly, this spatiotemporal coherence is even larger, and the highest in SWS (see Figs.4,S5,S6). Similarly, we found that during SWS, FS cells are phase-locked with LFP over up to 3 mm, while this phase-locking remains local during wakefulness. In contrast, RS cells show diminished spatial coherence during SWS and no significant correlation with distant LFP sites during wakefulness (Fig.4). The coherence of fast oscillations during SWS, that occur focally or over a span of few millimeters, poses a nice challenge for future modeling and experimental studies. A possible role of slow waves in memory consolidation has been well explored in the past decade (50; 51; 9). The present findings of similar fast oscillations during SWS and wakefulness are compatible with a reactivation of wake patterns. The higher coherence of SWS fast oscillations could perhaps be a substrate to induce long-term changes in cortical circuits during this reactivation. Such a possible role for fast oscillations in memory consolidation during sleep would be an interesting venue to explore.

Finally, slow oscillations show traveling waves over long distances (spanning several centimeters) during sleep (52). However, much of the information about traveling waves is based on studies in anesthetized animals (53; 54; 55). Although recent developments in multi-electrode array recordings technology have enabled the detection of (γ) fast oscillatory waves in anesthetized preparations (56), it is only recently that traveling β waves have been reported in the awake state (57; 58). In a recent study it was shown that the anisotropy of the cortical wiring may influence the spatiotemporal spike patterning (at least in the motor cortex) and that FS cells

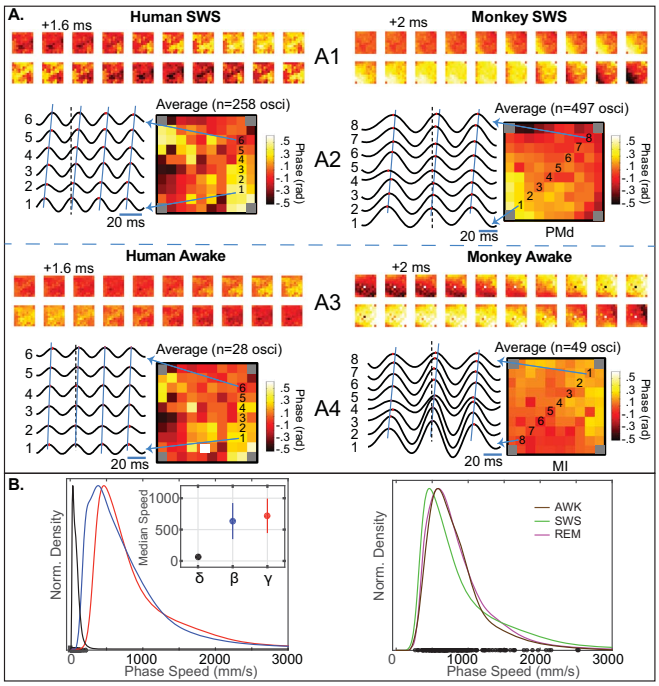

FIG. 5.— **A. Wave propagation in the δ (0.5-4 Hz) γ (30-50 Hz) and β (15-30 Hz) frequency range during SWS or wakefulness.** LFPs in the γ and β band from a single trial are plotted with respect to the spatial arrangement of the recording electrodes. A1,A3) Spatiotemporal plots of example LFP waves in human (left) and monkey (right) for both SWS (A1) and wakefulness (A3). A2,A4). **B. Phase speed distributions across frequency bands and across network states.** Plotted are the kernel smoothing density estimates for delta (δ), beta (β), and gamma (γ) frequency bands, during SWS (left panel). Speed estimates from individual delta epochs are plotted on the abscissa (black dots). Propagation in the delta frequency band exhibited speeds predominantly in the 10-100 mm/s range, while β and γ frequency propagation exhibited higher speeds (median + median absolute deviation, inset). γ oscillations across different states exhibited similar distributions of propagation speed (right panel). Speed estimates from individual -epochs in the awake state are plotted on the abscissa (black dots). AWK, awake; Norm., normalized.

were found to fire more reliably in phase with the β oscillation (59). In the present paper, we adapted a phase-based method (60) to detect propagating fast oscillatory waves, and found that both wakefulness and sleep harbor these waves (Fig.5) and that their speed is not affected by the state of consciousness. However, they do exhibit a tendency to manifest stereotypical directionality (see Fig.5, and supplementary movies). Dominant directionality could be related to the underlying connectivity profile that serves the intra- and inter-cortical information transfer (57). The computational implication of horizontal connections could point to a preset preferred path for information processing within a given functional domain of the neocortex (61; 62; 60). That such directional path is "functionally" preserved in sleep could be a further evidence that corticothalamic UP states replay fragments of wakefulness (63). The fast oscillations dynamics that we found here is consistent with such reactivation.

CONCLUSION

These findings confirm and extend earlier studies reporting high-frequency oscillations (>20 Hz) during sleep (11; 4; 6). In particular, we found that β and γ oscilla-

tions organize and modulate cortical population activity during SWS in the form of coherent waves traveling over several millimeters in the human/monkey neocortex. In addition, we observed that FS cells are strongly involved in the generation of these spatiotemporal patterns. The partial overlap between the spatial distribution of β/γ oscillations during sleep and wakefulness (57) suggests that these waves share similar functional attributes. During sleep, they may replay wake patterns with increased coherence that could play a role in memory consolidation.

METHODS SUMMARY

In epileptic humans with intractable seizures, 10x10 multielectrode arrays (400 μm inter-electrode separation, 1.0 mm electrode length) were implanted in the middle temporal gyrus. Patients consented to the procedure that was approved by the MGH (Massachusetts General Hospital) ''Institutional Review Board" in accordance with the ethical standards of the Declaration of Helsinki. In monkey, similar arrays were implanted in MI and PMd. The procedure was approved by the University of Chicago's IACUC and conform to the principles outlined in the ''Guide for the Care and Use of Laboratory Animals" (NIH publication no. 86–23, revised 1985). Details of cell categorization, β and γ event detection, synchrony and analysis of spatiotemporal activity patterns are provided in (64; 65; 11; 12; 66; 60; 13) and the supplementary material.

Research was funded by Harvard's Wyss Institute for Biologically Inspired Engineering; Agence Nationale de le Recherche ANR-10-IAIHU-06; Centre National de la Recherche Scientifique, European Community Future and Emerging Technologies program (BrainScales FP7-269921; The Human Brain Project FP7-604102), ONR (MURI award N00014-13-1-0672) and NIH grants 5R01NS062092, R01EB009282, R01NS045853 and R01MH099645. LM was supported by an NIH training grant (5T32EY20503-5). We thank Zach Haga for monkey data collection.

REFERENCES

[1]Brovelli A et al. (2004) Beta oscillations in a large-scale sensorimotor cortical network: Directional influences revealed by Granger causality. *Proc Natl Acad Sci U.S.A* 101(26):9849–9854.

[2]Donoghue JP, Sanes JN, Hatsopoulos NG, Gal G (1998) Neural discharge and local field potential oscillations in primate motor cortex during voluntary movements. *J Neurophysiol* 79:159–73.

[3]Fries P, Nikolić D, Singer W (2007) The gamma cycle. *Trends Neurosci* 30(7):309–316.

[4]Steriade M, Amzica F, Contreras D (1996) Synchronization of fast (30-40 Hz) spontaneous cortical rhythms during brain activation. *J Neurosci* 16:392–417.

[5]Steriade M, McCarley RW (2005) *Brainstem Control of Wakefulness and Sleep*. (Kluwer Academic, New York, USA).

[6]Destexhe A, Contreras D, Steriade M (1999) Spatiotemporal analysis of local field potentials and unit discharges in cat cerebral cortex during natural wake and sleep states. *J Neurosci* 19:4595–4608.

[7]Clemens Z et al. (2007) Temporal coupling of parahippocampal ripples sleep spindles and slow oscillations in humans. *Brain* 130(11):2868–2878.

[8]Buzski G (1998) Memory consolidation during sleep: a neurophysiological perspective. *J Sleep Res* 7 Suppl 1:17–23.

[9]Diekelmann S, Born J (2010) The memory function of sleep. *Nat Rev Neurosci* 11:114–126.

[10]Llinas R, Ribary U (1993) Coherent 40-Hz oscillation characterizes dream state in humans. *Proc Natl Acad Sci U.S.A* 90(5):2078–2081.

[11]Le Van Quyen M et al. (2010) Large-scale microelectrode recordings of high-frequency gamma oscillations in human cortex during sleep. *J Neurosci* 30(23):7770–7782.

[12]Peyrache A et al. (2012) Spatiotemporal dynamics of neocortical excitation and inhibition during human sleep. *Proc Natl Acad Sci U.S.A* 109:1731–6.

[13]Dehghani N et al. (2016) Dynamic balance of excitation and inhibition in human and monkey neocortex. *Sci Rep* 6:23176.

[14]Bazhenov M, Timofeev I (2006) Thalamocortical oscillations. *Scholarpedia* 1(6):1319.

[15]Haider B, Duque A, Hasenstaub AR, McCormick DA (2006) Neocortical network activity in vivo is generated through a dynamic balance of excitation and inhibition. *J Neurosci* 26(17):4535–4545.

[16]Csicsvari J, Jamieson B, Wise KD, Buzsáki G (2003) Mechanisms of gamma oscillations in the hippocampus of the behaving rat. *Neuron* 37(2):311–322.

[17]Hjos N et al. (2004) Spike timing of distinct types of GABAergic interneuron during hippocampal gamma oscillations in vitro. *J Neurosci* 24(41):9127–9137.

[18]Sohal VS, Huguenard JR (2005) Inhibitory coupling specifically generates emergent gamma oscillations in diverse cell types. *Proc Natl Acad Sci U.S.A* 102(51):18638–18643.

[19]Quilichini P, Sirota A, , Buzski G (2010) Intrinsic circuit organization and theta-gamma oscillation dynamics in the entorhinal cortex of the rat. *J Neurosci* 30(33):11128–11142.

[20]Atallah BV, Scanziani M (2009) Instantaneous modulation of gamma oscillation frequency by balancing excitation with inhibition. *Neuron* 62(4):566–577.

[21]Whittington MA, Traub RD, Kopell N, Ermentrout GB, Buhl EH (2000) Inhibition-based rhythms: experimental and mathematical observations on network dynamics. *International Journal of Psychophysiology* 38(3):315–336.

[22]Traub RD, Whittington MA, Jefferys JG (1999) *Fast oscillations in cortical circuits*. (MIT Press, Cambridge, USA).

[23]Buchsbaum M et al. (1982) Topographic cortical mapping of EEG sleep stages during daytime naps in normal subjects. *Sleep* 5:248–55.

[24]Steriade M (2006) Grouping of brain rhythms in corticothalamic systems. *Neuroscience* 137(4):1087–1106.

[25]Ayoub A, Mlle M, Preissl H, Born J (2012) Grouping of MEG gamma oscillations by EEG sleep spindles. *Neuroimage* 59(2):1491–1500.

[26]Valencia M, Artieda J, Bolam JP, Mena-Segovia J (2013) Dynamic interaction of spindles and gamma activity during cortical slow oscillations and its modulation by subcortical afferents. *PLoS ONE* 8(7):e67540.

[27]Cantero JL, Atienza M, Madsen JR, Stickgold R (2004) Gamma EEG dynamics in neocortex and hippocampus during human wakefulness and sleep. *Neuroimage* 22(3):1271–1280.

[28]Valderrama M et al. (2012) Human gamma oscillations during slow wave sleep. *PLoS ONE* 7(4):e33477.

[29]Van Vreeswijk C, Abbott LF, Ermentrout GB (1994) When inhibition not excitation synchronizes neural firing. *J Comput Neurosci* 1(4):313–321.

[30]Destexhe A, Contreras D, Steriade M (1998) Mechanisms underlying the synchronizing action of corticothalamic feedback through inhibition of thalamic relay cells. *J Neurophysiol* 79:999–1016.

[31]Cardin JA et al. (2009) Driving fast-spiking cells induces gamma rhythm and controls sensory responses. *Nature* 459(7247):663–667.

[32]Buzski G, Wang XJ (2012) Mechanisms of gamma oscillations. *Annu Rev Neurosci* 35:203–25.

[33]Traub RD (2006) Fast oscillations. *Scholarpedia* 1(12):1764.

[34]Tiesinga P, Sejnowski TJ (2009) Cortical enlightenment: Are attentional gamma oscillations driven by ING or PING? *Neuron* 63(6):727–732.

[35]Roopun AK et al. (2006) A beta2-frequency (20-30 Hz) oscillation in nonsynaptic networks of somatosensory cortex. *Proc Natl Acad Sci U.S.A* 103(42):15646–15650.
[36]Buzsáki G, Draguhn A (2004) Neuronal oscillations in cortical networks. *Science* 304:1926–9.
[37]Buzsáki G (2006) *Rhythms of the Brain*. (Oxford University Press (OUP), New York, USA).
[38]Sejnowski TJ, Paulsen O (2006) Network oscillations: emerging computational principles. *J Neurosci* 26:1673–6.
[39]Maquet P (2001) The role of sleep in learning and memory. *Science* 294:1048–52.
[40]Sejnowski TJ, Destexhe A (2000) Why do we sleep? *Brain Res* 886:208–223.
[41]Steriade M, Timofeev I (2003) Neuronal plasticity in thalamocortical networks during sleep and waking oscillations. *Neuron* 37:563–76.
[42]Crunelli V, Hughes SW (2009) The slow ($\leq$1 Hz) rhythm of non-REM sleep: a dialogue between three cardinal oscillators. *Nat Neurosci* 13(1):9–17.
[43]Kopell N, Ermentrout GB, Whittington MA, Traub RD (2000) Gamma rhythms and beta rhythms have different synchronization properties. *Proc Natl Acad Sci U.S.A* 97(4):1867–1872.
[44]Kreiter AK, Singer W (1992) Oscillatory neuronal responses in the visual cortex of the awake macaque monkey. *Eur J Neurosci* 4:369–375.
[45]Murthy VN, Fetz EE (1996) Synchronization of neurons during local field potential oscillations in sensorimotor cortex of awake monkeys. *J Neurophysiol* 76:3968–82.
[46]Eckhorn R et al. (1988) Coherent oscillations: a mechanism of feature linking in the visual cortex? Multiple electrode and correlation analyses in the cat. *Biol Cybern* 60:121–30.
[47]Engel AK, Kreiter AK, Knig P, Singer W (1991) Synchronization of oscillatory neuronal responses between striate and extrastriate visual cortical areas of the cat. *Proc Natl Acad Sci U.S.A* 88:6048–52.
[48]Gray CM, Knig P, Engel AK, Singer W (1989) Oscillatory responses in cat visual cortex exhibit inter-columnar synchronization which reflects global stimulus properties. *Nature* 338:334–7.
[49]Steriade M, Contreras D, Amzica F, Timofeev I (1996) Synchronization of fast (30-40 Hz) spontaneous oscillations in intrathalamic and thalamocortical networks. *J Neurosci* 16:2788–808.
[50]Mlle M, Marshall L, Gais S, Born J (2004) Learning increases human electroencephalographic coherence during subsequent slow sleep oscillations. *Proc Natl Acad Sci U.S.A* 101:13963–8.
[51]Marshall L, Helgadttir H, Mlle M, Born J (2006) Boosting slow oscillations during sleep potentiates memory. *Nature* 444:610–3.
[52]Massimini M, Huber R, Ferrarelli F, Hill S, Tononi G (2004) The sleep slow oscillation as a traveling wave. *J Neurosci* 24(31):6862–6870.
[53]Bringuier V, Chavane F, Glaeser L, Frgnac Y (1999) Horizontal propagation of visual activity in the synaptic integration field of area 17 neurons. *Science* 283:695–9.
[54]Grinvald A, Lieke EE, Frostig ARD, Hildesheim R (1994) Cortical point-spread function and long-range lateral interactions revealed by real-time optical imaging of macaque monkey primary visual cortex. *J Neurosci* 14:2545–2568.
[55]Xu W, Huang X, Takagaki K, Wu Jy (2007) Compression and reflection of visually evoked cortical waves. *Neuron* 55:119–29.
[56]Gabriel A, Eckhorn R (2003) A multi-channel correlation method detects traveling gamma-waves in monkey visual cortex. *J Neurosci Methods* 131:171–84.
[57]Rubino D, Robbins KA, Hatsopoulos NG (2006) Propagating waves mediate information transfer in the motor cortex. *Nat Neurosci* 9(12):1549–1557.
[58]Takahashi K, Saleh M, Penn RD, Hatsopoulos NG (2011) Propagating waves in human motor cortex. *Front. Hum. Neurosci.* 5(40).
[59]Takahashi K et al. (2015) Large-scale spatiotemporal spike patterning consistent with wave propagation in motor cortex. *Nat Commun* 6:7169.
[60]Muller L, Reynaud A, Chavane F, Destexhe A (2014) The stimulus-evoked population response in visual cortex of awake monkey is a propagating wave. *Nat Commun* 5:3675.
[61]Gilbert CD (1992) Horizontal integration and cortical dynamics. *Neuron* 9(1):1–13.
[62]Ermentrout GB, Kleinfeld D (2001) Traveling electrical waves in cortex. *Neuron* 29(1):33–44.
[63]Destexhe A, Hughes SW, Rudolph M, Crunelli V (2007) Are corticothalamic 'up' states fragments of wakefulness? *Trends Neurosci* 30:334–42.
[64]Hatsopoulos NG, Geman S, Amarasingham A, Bienenstock E (2003) At what time scale does the nervous system operate? *Neurocomputing* 52-54:25–29.
[65]Le Van Quyen M, Bragin A (2007) Analysis of dynamic brain oscillations: methodological advances. *Trends Neurosci* 30(7):365–373.
[66]Dehghani N et al. (2012) Avalanche analysis from multielectrode ensemble recordings in cat monkey, and human cerebral cortex during wakefulness and sleep. *Front Physiol* 3(302).
[67]de la Rocha J, Doiron B, Shea-Brown E, Josić K, Reyes A (2007) Correlation between neural spike trains increases with firing rate. *Nature* 448(7155):802–806.
[68]Jacobs J, Kahana MJ, Ekstrom AD, Fried I (2007) Brain oscillations control timing of single-neuron activity in humans. *J Neurosci* 27(14):3839–3844.
[69]Kalaska JF, Cohen DA, Hyde ML, Prud'homme M (1989) A comparison of movement direction-related versus load direction-related activity in primate motor cortex, using a two-dimensional reaching task. *J Neurosci* 9:2080–102.
[70]Raos V, Franchi G, Vittorio Gallese LF (2002) Somatotopic organization of the lateral part of area F2 (dorsal premotor cortex) of the macaque monkey. *J Neurophysiol* 89(3):1503–1518.

Draft version August 4, 2016
Preprint typeset using LaTeX style emulateapj v. 12/16/11
1

doi:10.1073/pnas.1523583113

SUPPLEMENTARY INFORMATION: HIGH-FREQUENCY OSCILLATIONS IN HUMAN AND MONKEY NEOCORTEX DURING THE WAKE-SLEEP CYCLE

Michel Le Van Quyen †[1] Lyle E. Muller †[2] Bartosz Telenczuk †[3] Eric Halgren [4]
Syd S. Cash [5] Nicholas G. Hatsopoulos [6] Nima Dehghani ¶[7,8] Alain Destexhe ¶[3]
1. Centre de Recherche de l'Institut du Cerveau et de la Moelle pinire (CRICM), UPMC, France.
2. Computational Neurobiology Laboratory, Salk Institute, La Jolla, USA.
3. Laboratory of Computational Neuroscience, Unit de Neurosciences, Information et Complexit, CNRS, France.
4. Multimodal Imaging Laboratory, Departments of Neurosciences and Radiology, University of California San Diego, USA.
5. Department of Neurology, Massachusetts General Hospital and Harvard Medical School, USA.
6. Department of Organismal Biology and Anatomy, Committee on Computational Neuroscience, University of Chicago, USA.
7. Wyss Institute for Biologically Inspired Engineering, Harvard University, USA.
8. New England Complex Systems Institute, Cambridge, USA.

RECORDINGS

In epileptic humans with intractable seizures, 10x10 Neuroprobe silicon multielectrode arrays (Blackrock Microsystems, Salt Lake City, UT, USA) were implanted in the middle temporal gyrus. In both patients, the histological examination of the implanted tissue in the therapeutic resection, related the recording locations to the neocortical layers II/III. Continuous recordings in epilepsy monitorin unit were used for this study (48 hours/2 nights for patient 1 and 24 hours/1 night for patient 2). Electrode were implanted in regions expected to be removed and after the monitoring session, the impant area was excised. Patients consented to the procedure that was approved by the MGH (massachusetts general hospital) Institutional Review Board in accordance with the ethical standards of the Declaration of Helsinki. In monkey, similar arrays (UTAH array, 400 μm inter-electrode separation, 1.0 mm electrode length; BlackRock Microsystems, Inc., Salt Lake City, UT, USA) were implanted in MI and PMd. In PMd, 96 electrodes and in MI, 32 electrodes were recorded. Based on histological analysis of PMd (70), a depth of 1 mm from the pial surface will likely be targeting deep portions of layers II/III. Based on histological analysis of MI (69), a depth of 1 mm from the pial surface in MI will be targeting layers II/III. Data were recorded continuously for each night for two nights in a row; awake data were collected in the day between these nights. The procedure was approved by the University of Chicago's IACUC and conform to the principles outlined in the Guide for the Care and Use of Laboratory Animals (NIH publication no. 86–23, revised 1985). For more details on procedures see (66).

PATIENTS

Patient 1 Was a 52-year-old right-handed woman at the time of a continuous eight-day phase II video-invasive EEG monitoring study. The patient had a history of complex partial seizures with occasional secondary generalization beginning at the age of four and typically suffered from 10 - 15 events per day. Her seizures usually presented with sudden speech arrest associated with confusion and repetition of activities. MRI showed a region of encephalomalacia in the left temporo-occipital region. The NeuroPort microelectrode array was placed in the middle temporal gyrus. The distance to the nearest ECoG electrode where seizure onsets were detected was ∼2 cm. At the conclusion of the study, the patient underwent resection of the left anterior temporal lobe. Pathology showed hippocampal sclerosis with secondary cortical gliosis but not in the region around the microelectrode array. The patient remained seizure free for one year after the resection, but seizures returned after this period.

Patient 2 - was a 24-year-old right-handed woman at the time of a continuous four-day phase II video-invasive EEG monitoring study. Her seizures tended to present with staring spells, gulping sounds, a general feeling of heat, and hand automatisms which began around age fourteen. EEG monitoring from a Phase I study suggested that these seizures originated from the left anterior temporal region. MRI showed a large lesion in the left temporal lobe, believed to be a glioma. In accordance with the above findings, the patient was implanted with a combination of subdural and depth electrodes focused on the left temporal region. The NeuroPort research electrode was placed in the middle temporal gyrus about 2 cm posterior to the temporal tip. The distance to the nearest ECoG electrode where seizure onsets were detected was ∼4 cm. At the conclusion of the study the patient underwent a left anterior temporal lobectomy, a left amygdalohippocampectomy, and a lesionectomy of the posterior temporal lobe. Pathology determined the lesion to be a low-grade glioneuronal tumor although the by MRI and histology the cortex underlying the microelectrode array did not appear abnormal. At last evaluation, 6 months post-operatively, the patient was seizure free.

SPIKE SORTING AND CELL CATEGORIZATION

After offline spike sorting based on PCA (principle component analysis), each cell's average spike waveforms were used to extract the half width of the extracellular positive deflection and the valley-to-peak parameter. Using a K-means algorithm, these average waveforms were

[1] †co-first, ¶: corresponding author. M.L.V.Q., N.D., and A.D. designed research; E.H., S.C., and N.G.H. performed experiments; M.L.V.Q., L.E.M., B.T., and N.D. analyzed data; and N.D. and A.D. wrote the paper.
nima.dehghani@wyss.harvard.edu, destexhe@unic.cnrs-gif.fr

further clustered into two distinct groups. Cross correlation between cell pairs was used to detect interactions indicative of putative monosynaptic connections. This combined morpho-functional characterization of cells was used to categorize them as putative excitatory (regular spiking, RS) and putative inhibitory (fast-spiking, FS) cells. Rigorous multivariable quantification and clustering was implemented to obtain robust cell categorization. Only the robustly categorized cells were included in the analyses (Patient 1: 68 RS & 23 FS neurons, Patient 2: 30 RS & 5 FS neurons, Monkey: 99 RS & 53 FS neurons). For more details, see supplementary material in refs. (12) and (13).

AUTOMATIC DETECTION OF HIGH-FREQUENCY OSCILLATION AND TIME-FREQUENCY DECOMPOSITION

Hilbert transform was used to extract the envelope of the filtered LFP between 15-30 and 30-50 Hz for β and γ respectively. Oscillatory events were detected as significant deviations of the envelope average over the 96-electrode array in these specified frequency ranges. These events had to be longer than a minimal duration (i.e. 75 msec for γ oscillations). Amplitude of these oscillatory events had to pass the mean envelope $\pm$ 2 standard deviations in the corresponding frequency band over the entire period of recording. The oscillatory events were visually confirmed and included in the analyses only if they did not contain any epileptic activity (in humans). Morlet wavelet was used for time-frequency decomposition and precise characterization of the mean frequency, the beginning, maximum amplitude, and onset and offset of each oscillation (65). These timing features were used for calculation of average time-frequency representations. For more details see ref. (11).

SPIKE AND LFP PHASE LOCKING

Morlet wavelet was used to calculate the power and oscillatory phase of the frequency ranges of β and γ. A neuron was considered phase locked to a given fast oscillation band, if the hypothesis of its LFP phase distribution circular uniformity was rejected (at p-value <0.05) based on a Bonferroni-corrected Rayleigh test. For more details of the methods, see refs. (68; 11).

SPIKE SYNCHRONY

For creating surrogate data, every spike (in a given spike series of a cell) was jittered. The value of jittering was randomly and independently selected from a uniform distribution between -100 to 100 msec. Realization of this procedure for 100 times provided the statistical basis ($p = 0.01$) for 99% confidence intervals in each bin. If the cross-correlogram surpassed this surrogate statistical threshold, coincident spiking were considered synchronous (for more details, see ref. (64)). Furthermore, in analysis of surrogate data, we used a large jitter window of 100 ms. Our results indicated that correlograms were not sensitive to the size of this window within a broad range (25100 ms). Finally, in order to avoid spurious detections associated with brief bursts of spikes, we compared measurements of correlation with those normalized by the geometric mean of each cell pairs average firing rates (67). Similar results were obtained, suggesting that our observations did not simply reflect the synchrony generated by bursts of activities.

SPATIOTEMPORAL DYNAMICS

As in previous work (57; 60), LFPs filtered in the frequency ranges for β and γ (8th-order Butterworth, forward-reverse in time) were transformed into a complex timeseries via the analytic signal representation. Detection of oscillatory events proceeded as before (3 standard deviations for 100 ms). Detection of wave-like spatiotemporal organization within these oscillatory events followed an algorithmic approach modified from the phase-latency method for analysis of optical imaging data introduced in (60). Instantaneous speed was calculated as in ref. (57).

REFERENCES

[1]See the full reference list in the main article.

State	Mean amplitude (μV)	N (events)
Human WAKE γ	16.3±9.5	188
Human REM γ	20.0±16.4	1316
Human SWS γ	30.7±19.1	1865
Monkey WAKE β	29.5±11.0	3240
Monkey SWS β	35.0±17.5	8543

TABLE S1: **State-dependent oscillation amplitude.** For each state-oscillation category, mean amplitude and number of events are depicted above.

State	Peak frequency (Hz)	interval (sec)
Human WAKE γ	42.3±3.8	2.4±1.8
Human REM γ	41.6±4.1	2.4±1.8
Human SWS γ	40.9±4.0	2.4±1.9
Monkey WAKE β	24.6±2.9	1.3±0.7
Monkey SWS β	22.8±3.6	1.6±1.1

TABLE S2: **State-dependent peak frequency.** For each state-oscillation category, peak frequency and inter-episode interval are depicted above.

State	FS	RS
Human WAKE	6.4±12.7(0 – 57.0)	2.6±3.1(0 – 15.3)
Human REM	8.1±8.0(0.36 – 32.0)	2.1±2.0(0.03 – 10.4)
Human SWS	7.5±9.3(0.2 – 40.9)	1.9±2.0(0.03 – 14.1)
Monkey WAKE	9.4±7.4(0.6 – 31.1)	5.9±4.(0.25 – 20.5)
Monkey SWS	8.7±8.4(0.5 – 37.6)	3.5±2.6(0.1 – 12.1)

TABLE S3: **State-dependent firing rate (Hz).** For each state-cell category, firing rate's mean, std and range (in parenthesis) are depicted above.

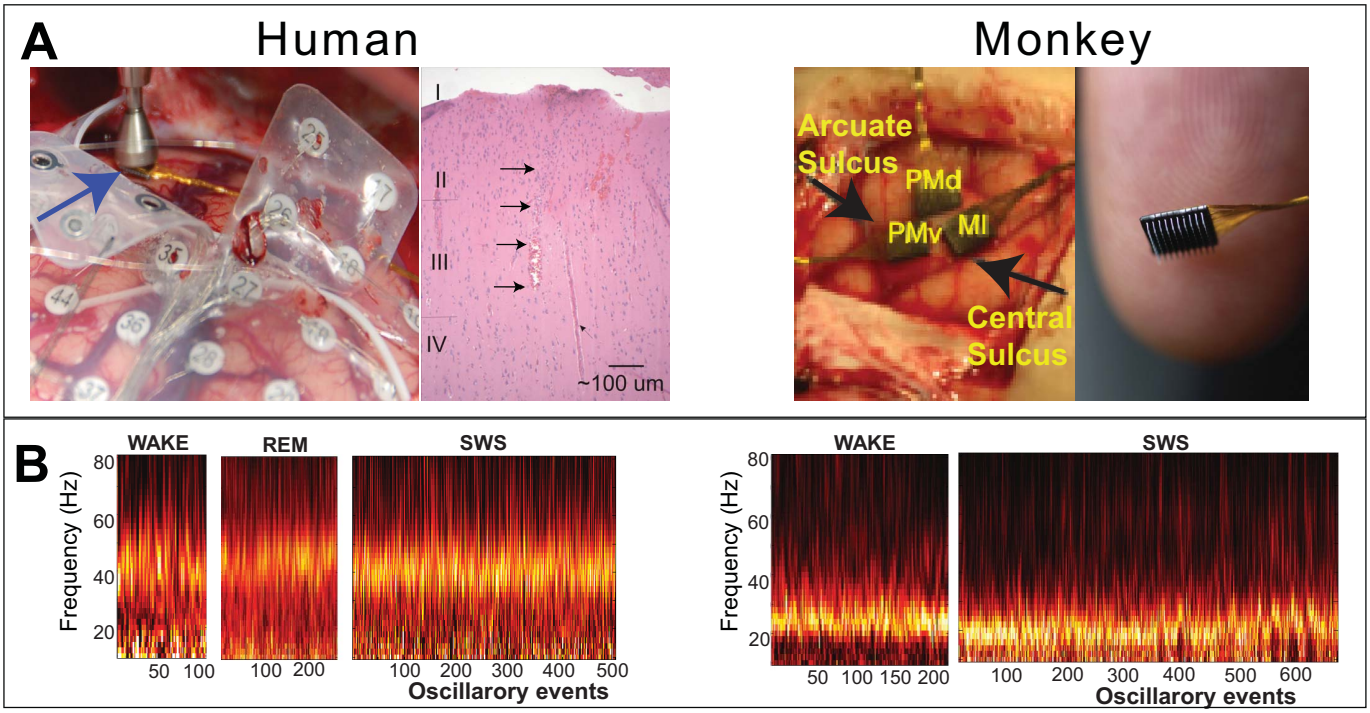

FIG. S1.—: **γ and β oscillations during sleep and wakefulness. (A)** Recordings from (44 mm) 100-electrode Utah (Neuroprobe) arrays are shown for neocortical γ oscillations in the temporal lobe of humans (left) and β oscillations in the dorsal pre-motor (PMd) and the motor cortex (MI) of monkey (right). Left: The array is implanted using a pneumatic device (blue arrow) under ECOG (electrocorticogram) macro-grid. The histology shows that array tract penetrates at least as far as superficial layer III. GFAP (glial fibrillary acidic protein) staining highlights focal gliosis of the superficial layers of the cortex. The NeuN (a neuronal specific nuclear protein) immunohistochemical staining reveals normal cortical layering with no evidence of cortical dysplasia. Right: Sleep recordings were from PMd and MI arrays and not ventral pre-motor (PMv). Scale of the array is shown in the far-right against fingertip. **(B)** Power spectra of few hundred examples of high-frequency oscillations during recorded vigilance states. Each column of the color-coded matrix is the average of time-frequency during an example epoch.

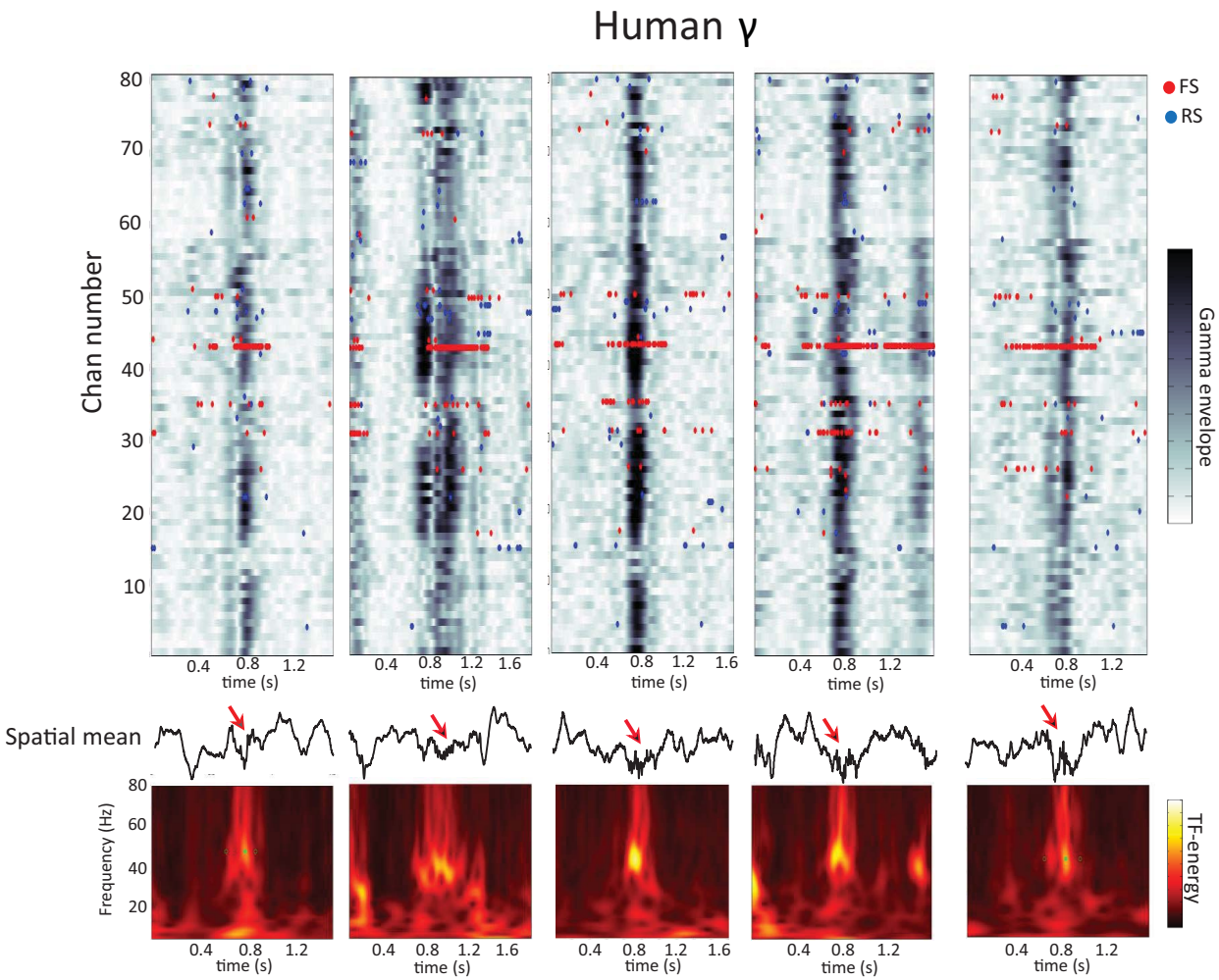

FIG. S2.—: **Examples of neocortical γ events in sleep.** Top panels show few example γ events from human patient 1. In these heatmaps, each row is a different LFP channel. Red and blue dots show spiking activity of FS and RS cells, localized at the same electrodes that were used to record the LFPs. Middle panels shows raw traces of average LFP recordings and the bottom panels show the wavelet time-frequency of the average LFP.

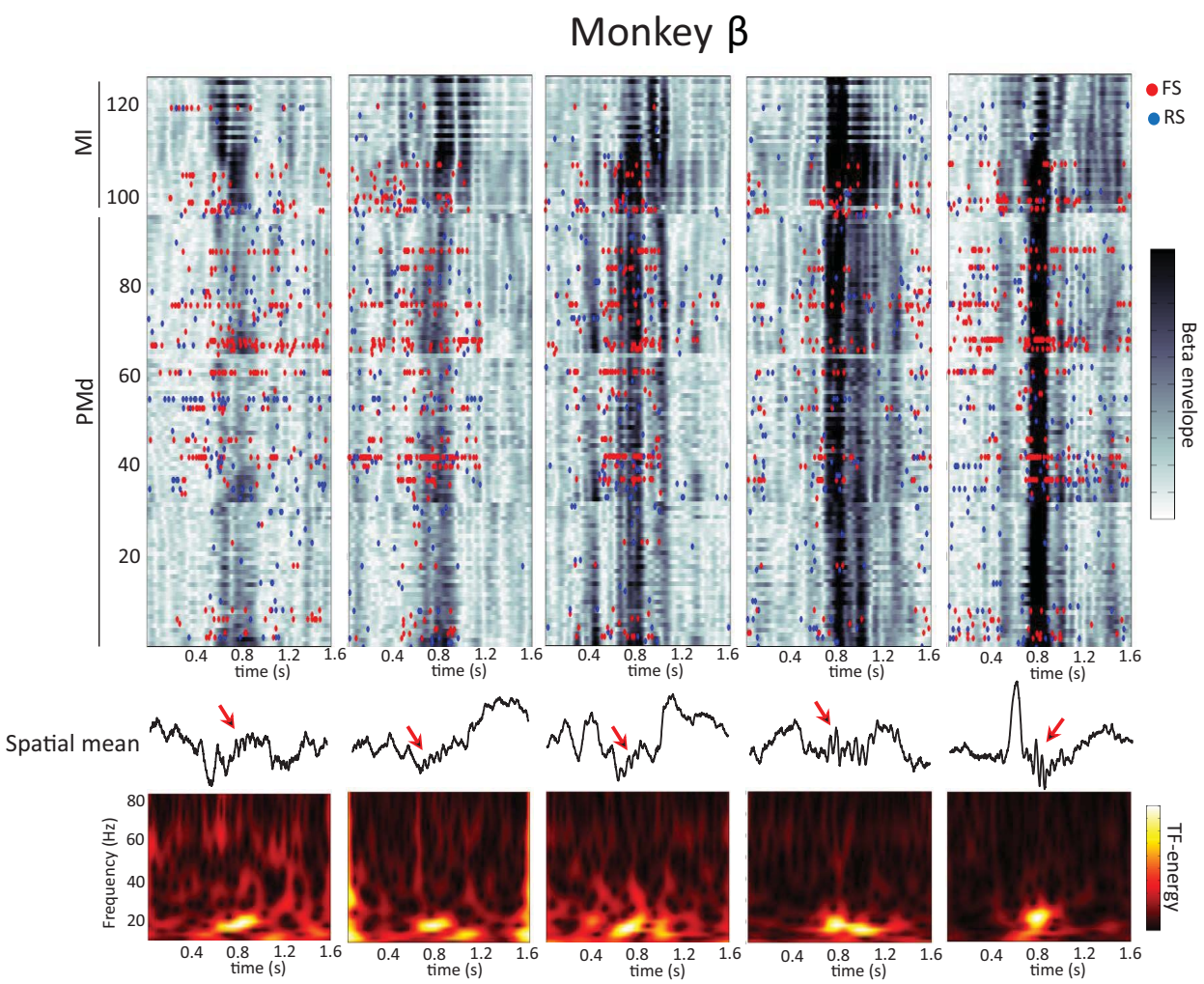

FIG. S3.—: **Examples of neocortical β events in sleep.** Top panels show few example β events from monkey. In these heatmaps, each row is a different LFP channel. Red and blue dots show spiking activity of FS and RS cells, localized at the same electrodes that were used to record the LFPs. Middle panels shows raw traces of average LFP recordings and the bottom panels show the wavelet time-frequency of the average LFP.

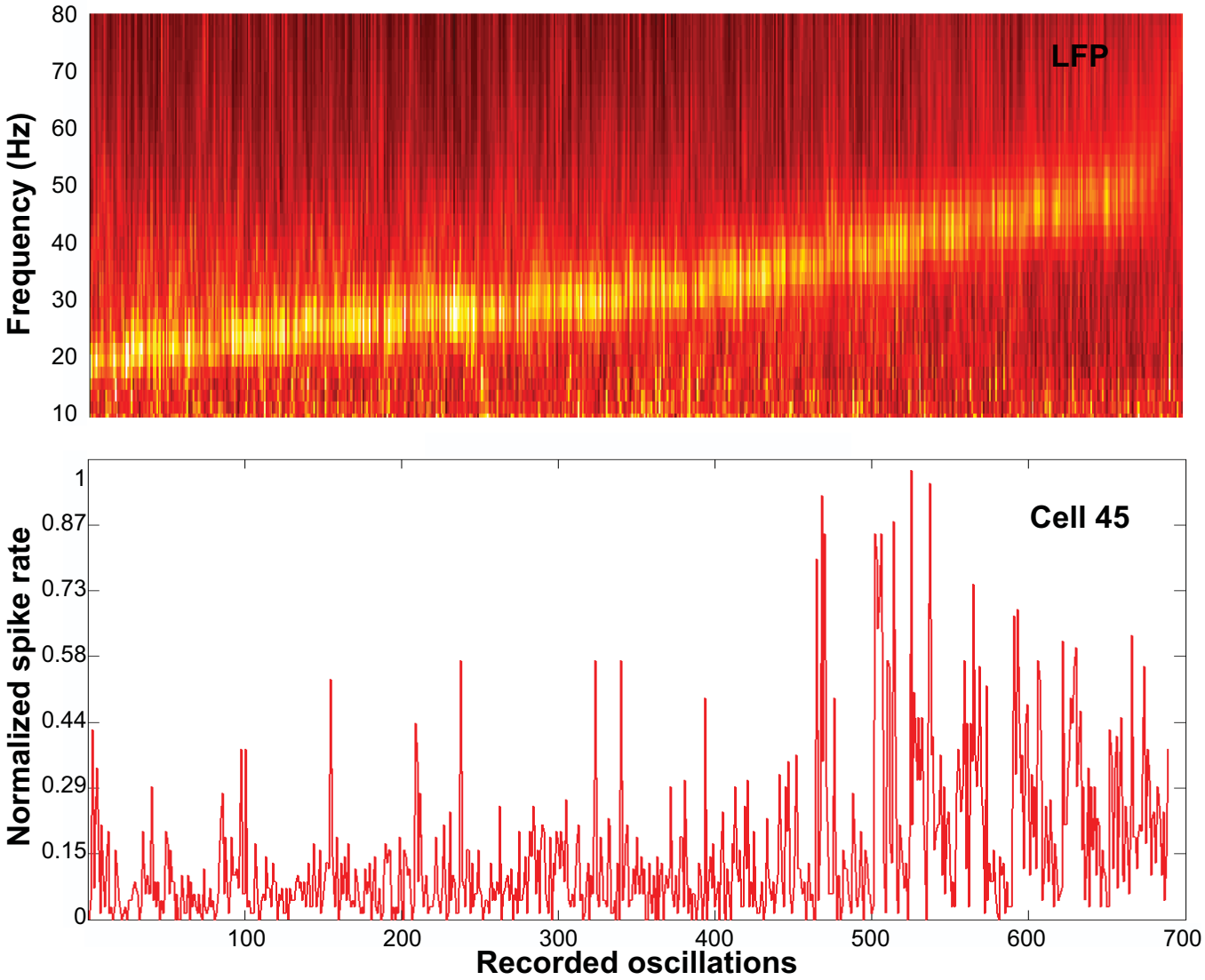

FIG. S4.—: **Oscillation-spiking relation.** In this example, ∼700 oscillatory events from a given channel were studied. The dominant oscillating frequency of these events were sorted from low to high (x axis, top panel, LFP). The corresponding normalized (to maximum) spike rate during each event of the recorded FS cell (from the same electrode) are shown in the bottom panel. This cell shows a clear higher spiking rate relationship during higher frequencies.

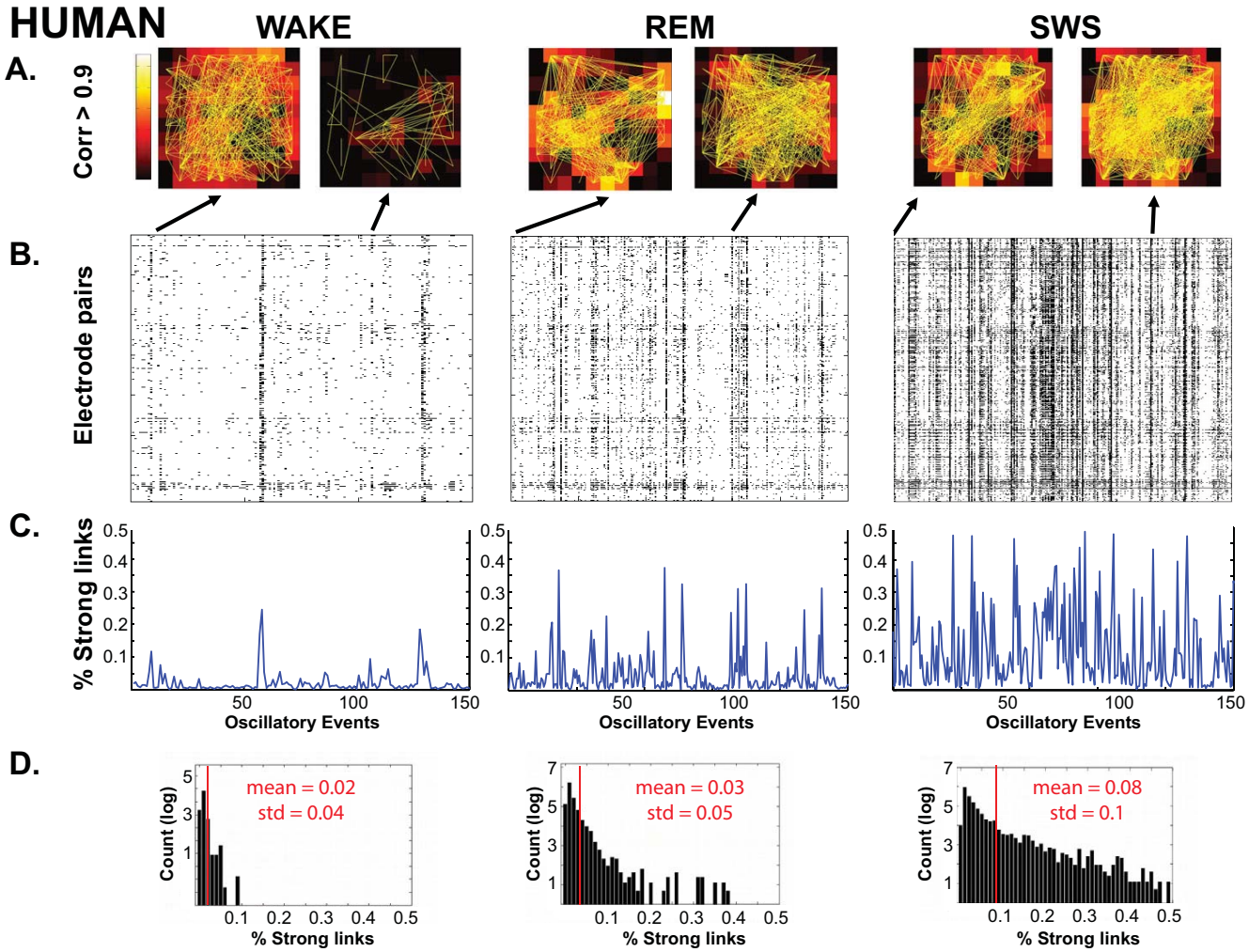

FIG. S5.—: **(A) Patterns of strong links** (max crosscorrelation ≥ 0.9 over a delay of ± 50 msec) occurring across the grid (human). (B) Patterns of pair-wise LFP spatial correlation for different states. Arrows point to the corresponding spatial profile of strong links at sample times. (C) Size distributions of the coherent patterns. In all states, widespread strong correlation across the grid can be seen, but they are less frequent during the wake state and very frequent during SWS. (C),(D) show the percentage and statistical distribution of strong links.

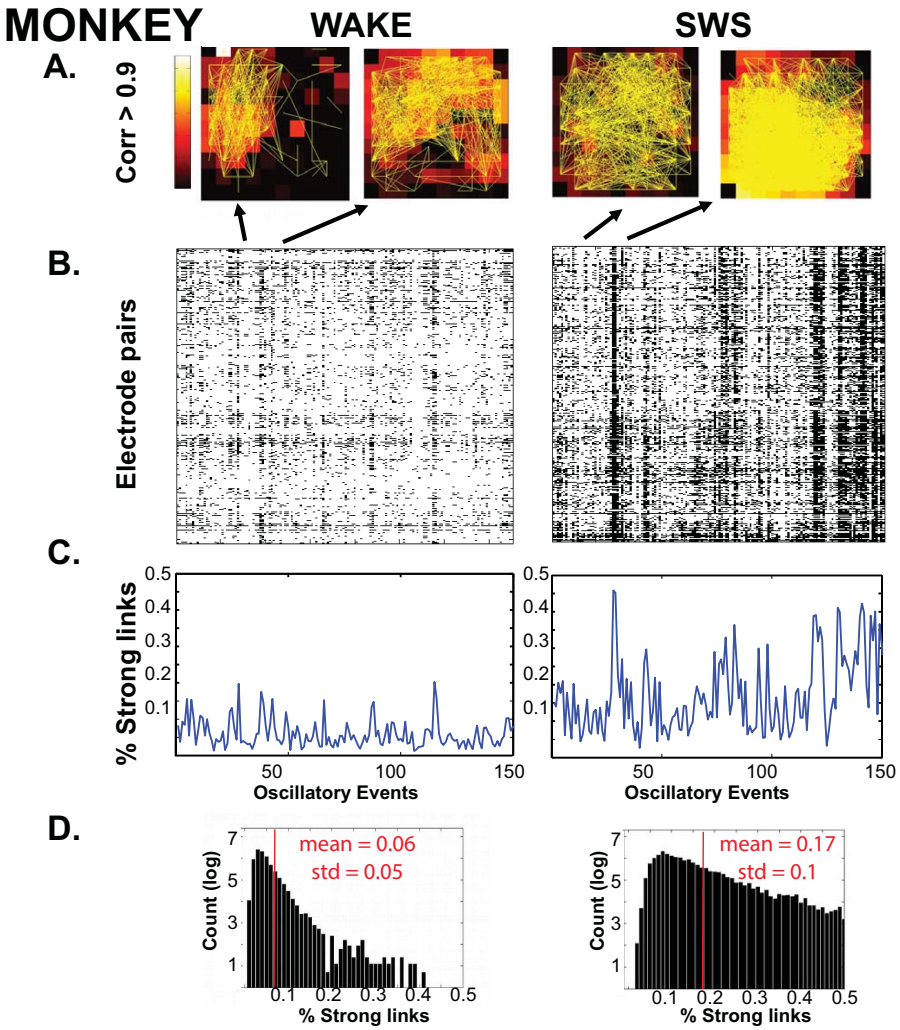

FIG. S6.—: **(A) Patterns of strong links** (maximum cross-correlation 0.9 over a delay of 50 ms) occurring across the grid (Monkey). (B) The spatial correlations are higher during SWS than during the wake state. Large patterns of strong links can mostly be seen during SWS. Similar observations can be made for human data (see Fig.S5). (C),(D) show the percentage and statistical distribution of strong links.

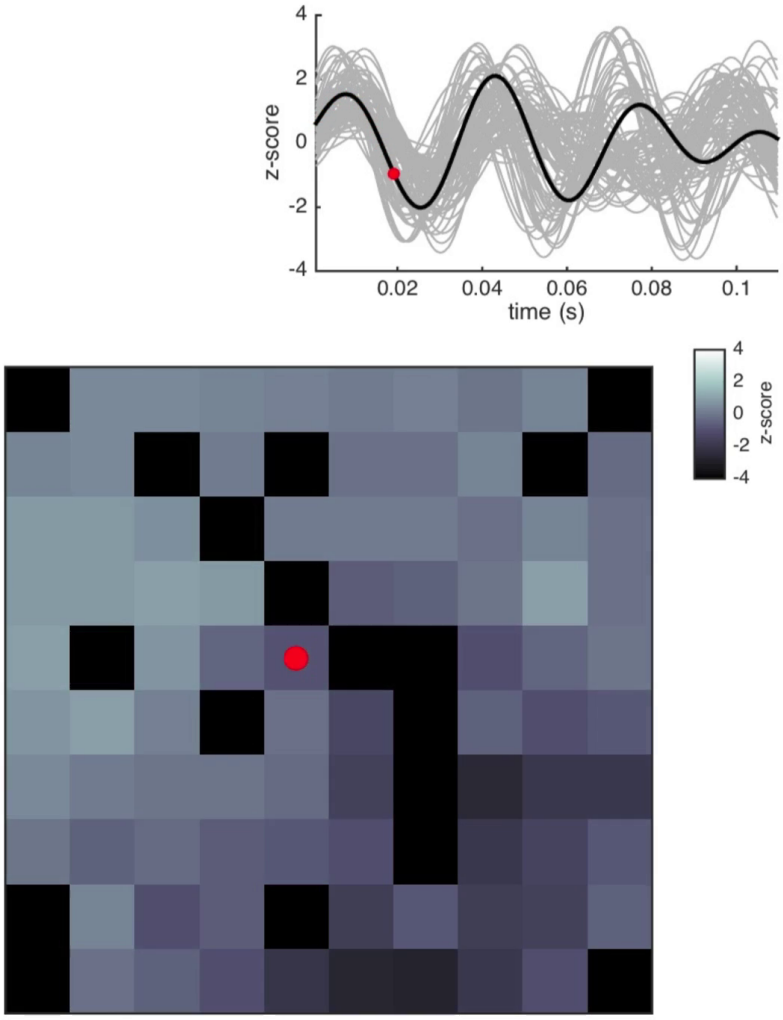

Spatiotemporal activity pattern in an example β-frequency wave in human SWS. In this movie, z-score amplitudes are plotted in false-color (bottom panel). In the top panel, the red dot traces out the timecourse of the channel in black (shown at its corresponding array position, below); all other channels are plotted in gray. For downloading the movie, see `dx.doi.org/10.1073/pnas.1523583113` supplementary information.

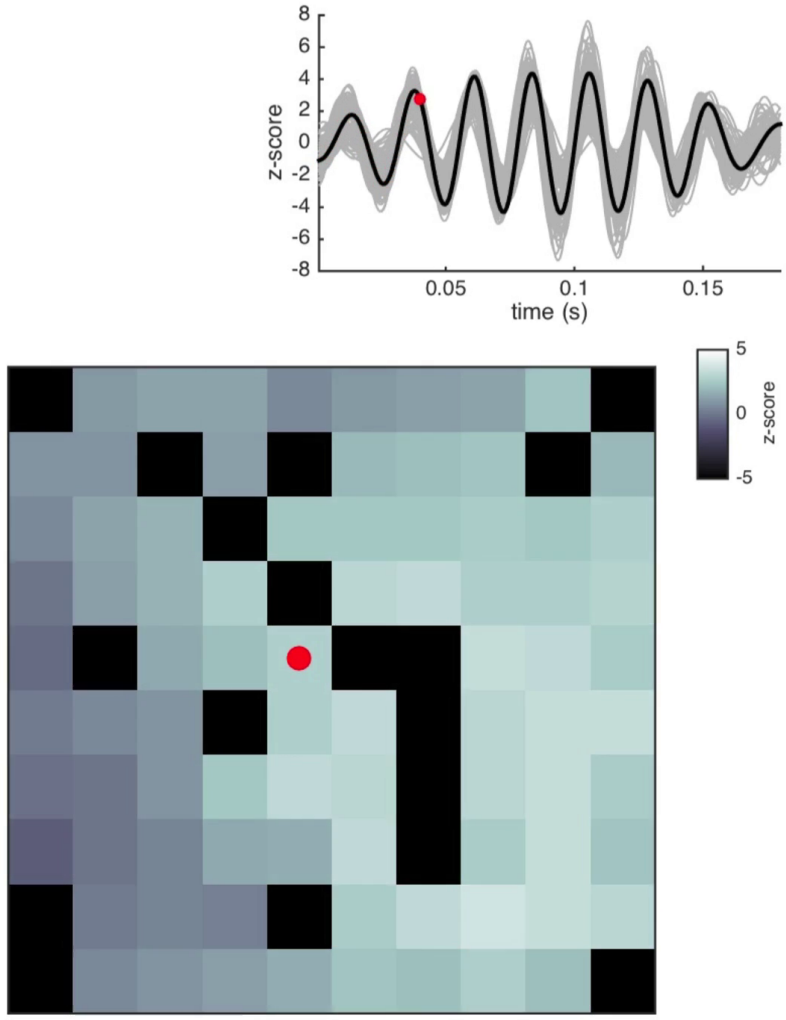

Example of a γ-frequency wave in human SWS. Data are plotted as in Movie S1. For downloading the movie, see `dx.doi.org/10.1073/pnas.1523583113` supplementary information.

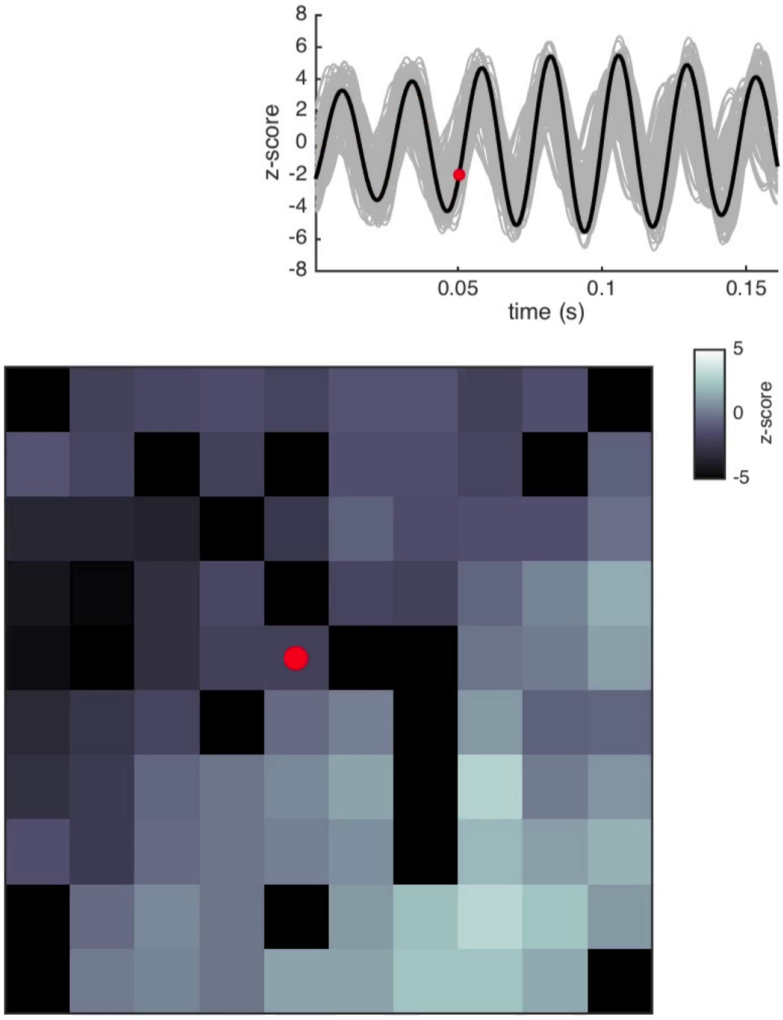

Additional example of γ-frequency wave in human SWS. Data are plotted as in Movie S1. For downloading the movie, see dx.doi.org/10.1073/pnas.1523583113 supplementary information.